Vilniaus universiteto
Fizikos fakulteto
Fotonikos ir nanotechnologijų institutas

Aleksandra Širvinskytė

PRIVERSTINĖ SPINDULIUOTĖ IR OPTINIS STIPRINIMAS InGaN DARINIUOSE

Bakalauro studijų baigiamasis darbas

Šviesos technologijų studijų programa

Studentas	Aleksandra Širvinskytė
Leista ginti	2023-01-11
Darbo vadovas	Dr. Jūras Mickevičius
Instituto atstovas	Dr. Dovydas Banevičius

Vilnius 2023

Vilnius University
Faculty of Physics
Institute of Photonics and Nanotechnology

Aleksandra Širvinskytė

STIMULATED EMISSION AND OPTICAL GAIN IN InGaN STRUCTURES

Bachelor's final thesis
Light Engineering study programme

Student	Aleksandra Širvinskytė
Approved	2023-01-11
Academic supervisor	Dr. Jūras Mickevičius
Representative of the Institute	Dr. Dovydas Banevičius

Vilnius 2023

TABLE OF CONTENTS

INTRODUCTION **4**

1. LITERATURE ANALYSIS **5**

1.1 OPTICAL EMISSION IN SEMICONDUCTORS 5

1.2 InGaN PROPERTIES 6

1.3 InGaN GROWTH ISSUES 7

1.4 POLARIZATION AND INTERNAL ELECTRIC FIELD 8

1.5 STIMULATED EMISSION IN InGaN 9

2. METHODOLOGY **10**

2.1 SAMPLES: InGaN STRUCTURES 10

2.2. PHOTOLUMINESCENCE SPECTROSCOPY 11

3. RESULTS **13**

3.1 EXCITATION-DEPENDENT PL MEASUREMENTS 13

3.2 MQWs 16

3.3 EPILAYERS 18

3.4. PEAK POSITIONS OF SP EMISSION AND SE BANDS 19

3.5 OPTICAL GAIN IN MQWs 20

4. CONCLUSIONS **23**

REFERENCES **24**

INTRODUCTION

InGaN ternary alloy semiconductors have attracted a lot of attention because of their numerous applications in optical and electrical devices as laser diodes (LDs), light-emitting diodes (LEDs), solar cells. Bandgap tunability by varying the amount of In in the compound or the width of the quantum well (QW) is one of the most appealing properties of InGaN structures and made InGaN/GaN multiple quantum wells (MQWs) indispensable in the field of solid-state laser sources. In particular, InGaN-based LDs were intensively studied as a promising laser source for high-density optical disk systems, full color displays, medical applications.[1–3]

Theoretically, InGaN could cover a broad spectral range from violet to near-infrared, however, alloys with high In content suffer from some growth issues such as large strain and defect formation due to differences in InN and GaN material properties, which consequently reduces efficiency of the device. Moreover, In compositional fluctuation and QW width fluctuation causes variations in the bandgap throughout the formed layer, all of which greatly influence radiative recombination rate and characteristics of LDs.[4] Therefore, recent studies are focused on optimizing the growth conditions of InGaN structures, understanding the peculiarities of stimulated emission (SE) process, optical gain in the ternary alloy and improving the stimulated efficiency while reducing the SE threshold.[2,5,6]

The main aim of this work is to study the influence of In content and/or QW width on the properties of stimulated emission in InGaN structures. To achieve this aim, the following tasks were formulated:

- Measure the excitation-dependent PL spectra of InGaN/GaN MQWs and epilayers in edge-emission configuration.
- Evaluate stimulated emission threshold in all studied structures and analyse its dependence on In content and/or QW width.
- Perform optical gain measurements using variable stripe length (VSL) technique and evaluate the gain coefficients in the InGaN MQW samples with different QW width.

1. LITERATURE ANALYSIS

1.1 OPTICAL EMISSION IN SEMICONDUCTORS

The main radiation processes in the direct bandgap semiconductors include absorption, spontaneous emission and stimulated emission illustrated in Fig. 1. Non-equilibrium carriers are generated when the electrons in the valence band (VB) are excited to the conduction band (CB) of the semiconductor. This process is initiated by irradiation of the sample with electromagnetic radiation of higher energy than the bandgap of the material. During the transition to the excited state both energy and momentum must be conserved. In direct bandgap semiconductors, the probability of a transition from VB to CB is high, although in indirect bandgap materials it is low due to the fact that it requires phonon assistance for the momentum conservation.

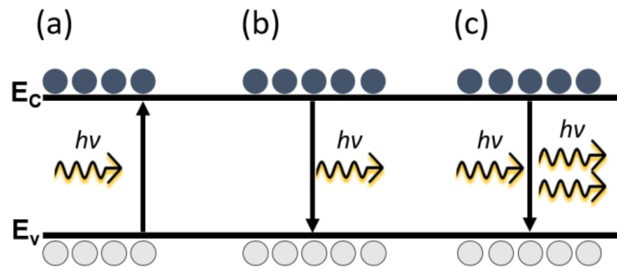

Fig. 1. (a) Absorption, (b) spontaneous emission, (c) stimulated emission.

The main radiative recombination mechanism responsible for optical emission in direct bandgap semiconductors is a band-to-band transition which corresponds to the transition between the excited state (conduction band) and the ground state (valence band). An electron in the conduction band recombines with the hole in the valence band emitting a photon. The photon is emitted in a random spatial direction and the resultant light wave has a random phase and polarization. This process is spontaneous and therefore is called spontaneous (SP) emission. However, if the energy of the incoming electromagnetic radiation matches the transition energy between the excited and the ground states, an incoming photon can provoke the photon emission. A provoked transition is called stimulated emission. In this case the emitted photon is of same energy and propagates in the same direction as the incoming photon and the corresponding light waves have the same phase and polarization. Optical amplification takes place only when a certain condition called population inversion is satisfied. This means that the number of electrons in the higher energy state has to exceed the number of electrons in the ground state, which is achieved by the supply of sufficient energy to the active medium.

However, carriers can also recombine through the non-radiative decay channels. Such recombination mechanisms include Shockley–Read–Hall (SRH) recombination and Auger recombination. SRH recombination is a process when an electron and a hole recombine through the

recombination center – localized state, which can also be called a trap. Origin of such energy states is usually a defect in the crystal lattice or a dopant. Traps can be located closer to VB or CB and are usually described by coefficients for the capture of electrons and holes. Firstly, an electron (or hole) gets trapped in the recombination center. Then the electron in the trap can be thermally re-emitted back to the CB or meet a hole and recombine generating a phonon. Auger recombination is a process, which involves three carriers. Here, electron and hole recombination results not in an emission of a photon or heat, but in energy transfer to the third particle – electron in the CB. This excess energy is later lost to thermal vibrations and electron relaxes to the lowest CB state.

1.2 InGaN PROPERTIES

InGaN is a ternary alloy composed of GaN and InN. GaN is a direct wide bandgap semiconductor material, which at ambient conditions has a hexagonal wurtzite crystal structure. However, GaN can also be grown in a cubic structure called zincblende.[7] Such layers have been achieved on cubic substrates (SiC, GaAs).[8,9] Zincblende crystals are characterized by one lattice constant as $a = b = c$ for cubic structure, while for wurtzite crystal a ($a = b$) and c lattice constants are used.[10]

InN is also a direct bandgap semiconductor, which can also be in a hexagonal or cubic form. The bandgap of InN at the temperature of 0 K was determined to be about 0.7 eV. In InN case, temperature-variation of the bandgap value is smaller (49 meV) than in other III-nitride compounds as GaN (72 meV) or AlN (92 meV).[11] Properties of InN and GaN are presented in Table 1.

Table 1. Binary III-nitride properties.

Semiconductor	Structure	Lattice constants (Å)	Bandgap (eV)
GaN	Wurtzite	$a = 3.189^a$ $c = 5.185^a$	$E_{g\ 295K} = 3.435^b$ $E_{g\ 0K} = 3.507^b$
InN	Wurtzite	$a = 3.545^a$ $c = 5.703^a$	$E_{g\ 295K} = 0.641^b$ $E_{g\ 0K} = 0.69^b$

a Reference [10];
b Reference [11].

As InGaN is a mixture of two materials, properties as bandgap and lattice constants greatly depend on the composition. InN being a small bandgap material allows altering the bandgap of InGaN (from 0.64 eV to 3.43 eV at 300 K) as well as the lattice constants. The change of these parameters can be described by the Vegard's law, however, while the change of lattice constants follows a linear relationship, bandgap dependence requires an additional bowing parameter accounting for the deviation from a linear interpolation.

1.3 InGaN GROWTH ISSUES

The major challenge in developing well-functioning optoelectronic devices is the growth of high quality MQWs. Growth of InGaN/GaN MQWs is most commonly performed by metal-organic chemical vapor deposition (MOCVD) and was extensively studied in the past decade.

The key to obtaining high quality InGaN/GaN MQWs is to choose the right growth parameters of the wells and the barriers. GaN is usually grown at relatively high temperatures (above 1000 °C[12]) to achieve good crystal quality. In case of InN growth, such temperatures would impede the formation of In clusters on the surface as InN has a low dissociation temperature of about 630 °C.[13] To achieve better quality of the InGaN/GaN MQWs, growth temperature of the wells has to be significantly lower than the temperature used to grow the GaN buffer layer or the barriers of MQWs. However, lower growth temperatures contribute to the ineffective dissociation of ammonia, which results in a lower amount of N radicals present to react with metallic In. The formation of In droplets could be suppressed by using large V/III ratios. In this case, sufficient amount of N is ensured.

To address the technical challenges described above and improve the crystalline quality of InGaN MQWs, growth interruption model was proposed. During the growth interruption Ga and In sources are closed while keeping continuous supply of ammonia. This leads to reaction between the In atoms on the surface of the grown layer and N radicals or desorption of In atoms from the surface due to thermal annealing.[14,15]

Group III nitrides are most commonly deposited on sapphire (Al_2O_3), silicon (Si), silicon carbide (SiC) or GaN substrates.[16] Different lattice parameters, thermal expansion coefficients of substrate and layer hinder the fabrication of strain-free structures, which intuitively makes GaN itself a preferable substrate choice. Unfortunately, due to high price and difficulties in obtaining large-size free-standing GaN wafers, GaN layers are usually grown on foreign substrates. Sapphire substrates are widely employed due to large wafer sizes, low cost and high quality of the wafers, however, they have a relatively high lattice mismatch with GaN (15%). The main drawbacks of the foreign substrates are induced strain, bowing of the wafer and defects.

The main types of defects found in InGaN/GaN QWs are threading dislocations, V-pit defects and deep level point defects that can act as a non-radiative centres and quench the PL due to enhanced non-radiative Shockley-Read-Hall recombination. This consequently reduces the PL efficiency of the structures. However, in case of low excitations, threading dislocations that end up in the V-pit defects can also lead to higher PL efficiencies due to self-screening of defects.[17] Carrier capture by such defects is inhibited due to potential barrier formed around the core.

1.4 POLARIZATION AND INTERNAL ELECTRIC FIELD

Both zincblende and wurtzite crystal structures have a noncentrosymmetric nature, which leads to a non-zero spontaneous polarization in the crystals. At the interface of two different materials a change of spontaneous polarization is present causing an internal electric field. Moreover, a large lattice mismatch between GaN and InN leads to a huge strain in InGaN layer, which induces a perturbation of the crystal lattice and causes the piezoelectric polarization. Therefore, a sum of spontaneous and piezoelectric polarizations has to be calculated to estimate the total polarization. In case of InGaN/GaN QWs, total polarization is mostly influenced by piezoelectric polarization as the difference between spontaneous polarization of GaN and InN is small (about 3 mC/m^2), while the lattice mismatch is large.[18]

Strong polarization in III-V nitrides induces an internal electric field, which greatly affects the properties of QWs. One of the effects observed is the tilt of conduction and valence bands inside the QW and consequent reduction of the band gap. This effect is called a quantum confined Stark effect (QCSE).[18] The shape of a QW changes from a square to a triangle, which causes spatial separation of the electron–hole wave functions to the sides of the well (Fig. 2.). Therefore, hole states are shifted to the higher energies while electron states to the lower energies, which results in a red shift of PL emission spectra and contributes to a decrease of PL intensity and radiative recombination due to the lower overlap of the electron-hole wave functions. The QCSE can be avoided if the MQWs are grown on a nonpolar plane or reduced if the width of the well is reduced, doping of barriers is performed or the strain is reduced in the QW.

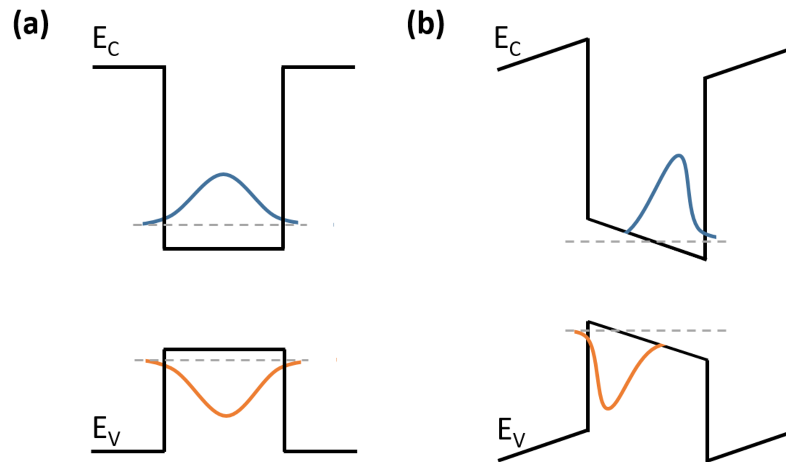

Fig. 2. QWs electronic band structure without (a) and with (b) electric field.

Based on ref. [18].

1.5 STIMULATED EMISSION IN InGaN

The first LD based on InGaN MQWs emitting at 417 nm was introduced back in 1996 by Nakamura S. *et al.*[19] Since then, InGaN-based LDs have been extensively studied and quickly improved. However, development of efficient longer wavelength LDs remains challenging due to InGaN growth issues, internal electric field, discussed in the previous chapters. Therefore, studies of SE in InGaN structures are focused on deeper understanding how the external conditions and sample parameters influence the SE parameters. One of the main SE parameters is a SE threshold which is defined as the lowest excitation density required to initiate the optical amplification. The SE band usually appears on the higher energy slope of the SP emission band in both InGaN/GaN MQW and InGaN epilayer structures.[20,21] This indicates that SE originates from the localized states.[22,23] Excitation-dependent PL measurements allow to compare the spectral shapes of SE and SP emission bands and evaluate the SE threshold. However, if measurements are performed at low temperatures, a clear change from SP emission band to SE band can be obscured due to low SE threshold at low temperatures.[23]

SE threshold was found to depend on the QW width and the amount of In in the alloy. One study showed that SE threshold decreases with increasing QW width up to 3.9 nm.[21] Such behavior was attributed to improved electron wave function confinement in the QW. However, S.K.Shee *et al.* used a time resolved photoluminescence (TRPL) technique for estimation of SE threshold and showed that once the QW width reaches 4.5 nm, SE threshold starts to increase rapidly.[24] It was suggested that high values of SE threshold for wide QWs (6 nm and 9 nm) could be a result of strain relaxation. It was also found that large In content (23 %) leads to larger SE threshold due to increased role of material inhomogeneities.[25]

Temperature dependent measurements of PL in InGaN structures generally reveal a characteristic S-shape peak position shift of the SP emission band.[26] The initial red shift of emission spectra appears due to carrier redistribution within the localized states via hopping. With further increase in temperature, carriers acquire enough thermal energy to occupy higher energy states, which results in the blue shift of PL peak position. This is followed by a second redshift induced by the bandgap shrinkage dominance.[27] A similar dependence was also found for SE in the InGaN epilayer, which was attributed to localization and thermal activation of nonequilibrium carriers.[23]

2. METHODOLOGY

2.1 SAMPLES: InGaN STRUCTURES

In this study, eleven InGaN/GaN MQWs samples and eight InGaN epilayer samples were studied. All studied samples were grown on sapphire substrate by metalorganic chemical vapor deposition (MOCVD) by J. S. Speck team at University of California, Santa Barbara. Investigated samples were composed of *n*-GaN buffer layer on top of which either InGaN epilayer or InGaN/GaN MQWs were grown. Protective GaN cap layer or AlGaN electron blocking layer was grown on top. The studied structures are schematically illustrated in Fig. 3.

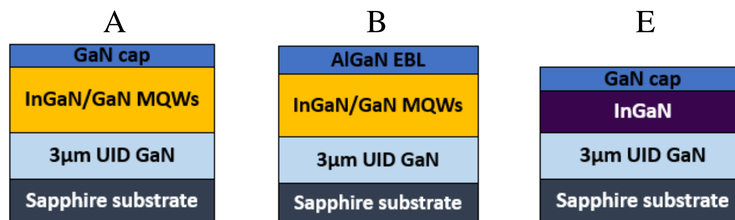

Fig. 3. Cross-sectional schematic diagram of InGaN/GaN structures.

Three sample groups are labeled based on their structure (A and B for MQWs and E for epilayers) and the varying parameter (In % or the QW width). The group A samples had a constant QW thickness (3 nm) and a different indium content, ranging from 9 % to 20 %. The MQWs in group B samples had constant indium content of 25 %, and different QW thickness, ranging from 1 nm to 4 nm. The thickness of InGaN epilayers was ~50 nm (except for the sample E8), while In content ranged from 3 % to 20 %. Parameters of each sample are presented in Table 2.

Table 2. Sample properties of MQW samples (a) and epilayer samples (b).

(a)

Sample name	Type	In content (In %)	QW (nm)
A1	MQWs	3	3
A2		9	3
A3		10	3
A4		12	3
A5		17	3
A6		20	3
B1		25	1
B2		25	1
B3		25	2
B4		25	2.7
B5		25	4

(b)

Sample name	Type	In content (In %)	QW (nm)
E1	Thick InGaN	3	54
E2		5	57
E3		9.3	45
E4		10	58
E5		12.1	46
E6		16.8	47
E7		19.9	50
E8		20.8	25

2.2. PHOTOLUMINESCENCE SPECTROSCOPY

Characterization of the samples was performed by the quasi-steady-state photoluminescence spectroscopy. Such technique is widely used due to versatility of the method, non-destructive approach, and the absence of sample processing needs. Measurements were performed under a wide range of excitation conditions (from 800 W/cm^2 to 21.7 MW/cm^2) at room temperature.

To detect SE, PL measurements were performed in an edge-emission configuration. In contrast to front-emission configuration, the laser beam is focused with a cylindrical lens into a narrow stripe (20 µm wide and 4 mm long) rather than a spot on the sample surface. As was discussed in chapter 1.1 spontaneous emission arises in random directions. Spontaneously emitted photons propagating along the stripe can provoke stimulated emission. Therefore, photons are detected from the edge of the sample. Such configuration is also needed for optical gain measurements where a VSL method[28] is used. The excitation stripe length is varied by a shifting razor blade, which works as a blocking screen. Measured emission spectra at different excitation stripe lengths allow to extract the optical gain coefficient or the gain spectrum.

Experimental setup used in this work is based on the third harmonic of the Nd:YAG laser as an excitation source, and a spectrometer (Andor Shamrock 500i) with an ICCD camera (Andor DH320T) as a detector. The detailed setup for the quasi-steady-state PL measurements is presented in Fig. 4.

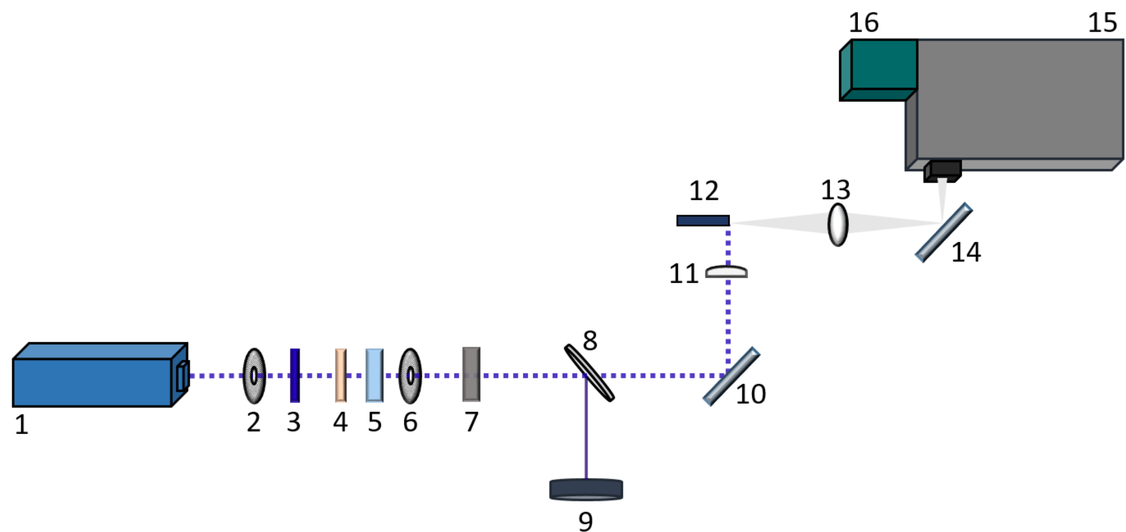

Fig. 4. Experimental setup for PL measurements. 1 – laser; 2 and 6 – pinhole; 3 – filter; 4 – polarizing half-wave plate; 5 – Glan prism; 7 – quartz cuvette with a solution of water and ink; 8 – beam-splitter; 9 – photodiode gauge; 10 and 14– mirrors; 11 – cylindrical lens; 12 – sample; 13 – spherical quartz lens; 15 – monochromator; 16 – ICCD camera.

The nanosecond laser (1) with a pulse duration of 4 ns, emitting radiation at 355 nm is used to excite the samples under study. Two pinholes (2) and (6) are used for spatial filtering and a colored glass filter (PS11) (3) is used to cut out the residual of the second harmonic of the Nd:YAG laser.

The excitation power is altered by the polarizing half-wave plate (4) while keeping the position of the analyzing Glan prism (5) constant. To reach the lowest excitations a quartz cuvette with a solution of water and ink was used (7) additionally. Part of the laser beam is deflected by a quartz plate beam splitter (8) to a photodiode gauge (9) for continuous monitoring of excitation. A cylindrical lens (11) is used to focus the laser beam onto the sample surface (12). A spherical quartz lens (13) is used to collect the PL signal from the sample edge onto the entrance slit of the monochromator (15). PL is detected by an ICCD camera (16).

3. RESULTS

3.1 EXCITATION-DEPENDENT PL MEASUREMENTS

To study SP emission and SE in InGaN structures, PL spectra of all samples under study were measured under a wide range of excitation power densities. Fig. 5 shows the excitation-dependent PL spectra of sample A4. At lowest excitations a broad SP emission PL band is observed. As the excitation power density is increased, the PL band blueshifts. This is caused by the band-filling effect and screening of the piezoelectric field. As more carriers are injected into the system, a higher-energy localized states are populated leading to the emission of higher-energy photons. In addition, high nonequilibrium carrier densities screen the built-in electric field and gradually change the shape of the QW back to the rectangular form. Consequently, the hole states are shifted to the lower energies, while the electron states to the higher energies, which contributes to the blue shift of PL emission spectra.[29] At the critical excitation power density, a second band appears on the high-energy slope of the spontaneous PL band peak. The intensity of the second band rapidly increases with further increase of excitation and shifts to lower energies. The redshift is a result of the bandgap renormalization caused by the many-body interactions of nonequilibrium carriers.[30] A narrow bandwidth and a rapid increase of PL intensity indicate that the second band arises due to stimulated emission. For the sample A4, the SE band appears at excitation power density of 144 kW/cm^2. At the same excitation power density, a sudden change in the behaviour of the PL efficiency (defined as the ratio of integrated PL intensity and the corresponding excitation power density) is observed (see the inset of Fig. 5). Such behaviour was evidenced for most of the samples under study. Therefore, the SE threshold is defined to be between the highest excitation power density at which only spontaneous PL band is observed and the lowest excitation power density at which the SE band appeared. The SE threshold of 126.2 kW/cm^2 was found for the sample A4, which is the lowest SE threshold of all samples under study.

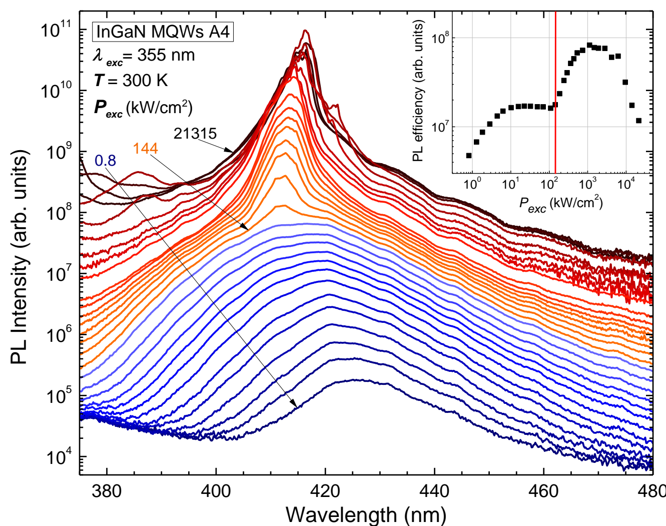

Fig. 5. Excitation-dependent PL spectra of the sample A4. Inset of the graph shows the PL efficiency dependence on the excitation power density.

Fig. 6 presents the SP emission spectra (Fig. 6(b)) and the SE spectra (Fig. 6(a)) of samples from groups A and E measured at the excitation power density below and above the SE threshold, respectively. Samples E6, E7 and E8, which had the highest content of In, showed no SE band even at the highest excitation conditions, therefore, their PL spectra are not shown in Fig. 6. The peak positions of the PL spectra are distributed over a wide range of wavelengths, ranging from 370 nm to 470 nm. It can be clearly seen that with increasing In content in the sample, the position of PL band peak shifts to longer wavelengths and the band broadens. The PL band peak position shift is caused by a smaller bandgap of InN compared to GaN. In addition, larger In content in the samples leads to larger variations in local composition, as well as stronger carrier localization resulting in the increased density of the localized states below the CB or above the VB causing PL band broadening.

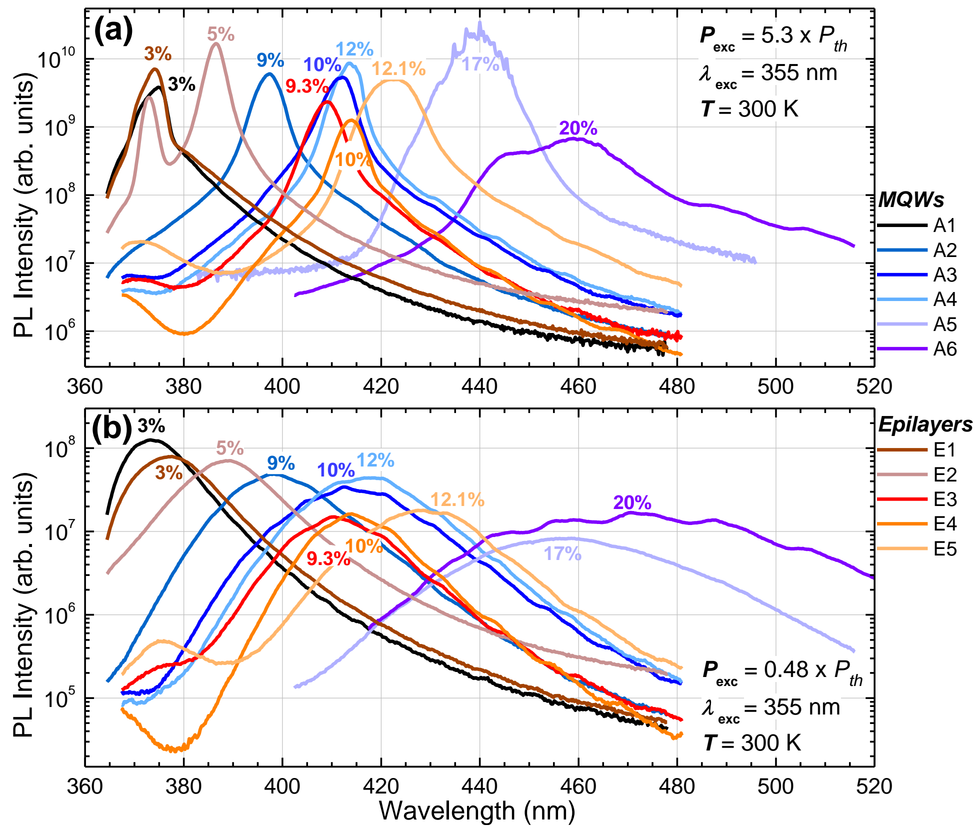

Fig. 6. PL spectra of the studied samples from groups A and E under excitation power density above (a) and below (b) SE threshold. Next to each of the spectra an indium content in the according sample is provided.

The PL spectra of the group B samples with different QW width are shown in Fig. 7. Results show that increasing QW width results in a red shift of emission spectra and a decrease in PL intensity when the excitation power density is below the SE threshold. The red shift can be attributed to the quantum confinement.[18] In case of larger QW widths the first quantum confined energy level forms closer to the conduction band (closer to the valence band in case of holes), therefore, emission is of lower energy. Decrease of PL intensity with increasing QW width could be explained in terms of

piezoelectric field. Larger QW widths result in a more significant influence of the piezoelectric field. When the excitation power density is below the SE threshold, the piezoelectric field is only partially screened, therefore, PL bands of the samples with larger QW widths are of lower intensity due to a lower overlap of the electron and hole wave functions.

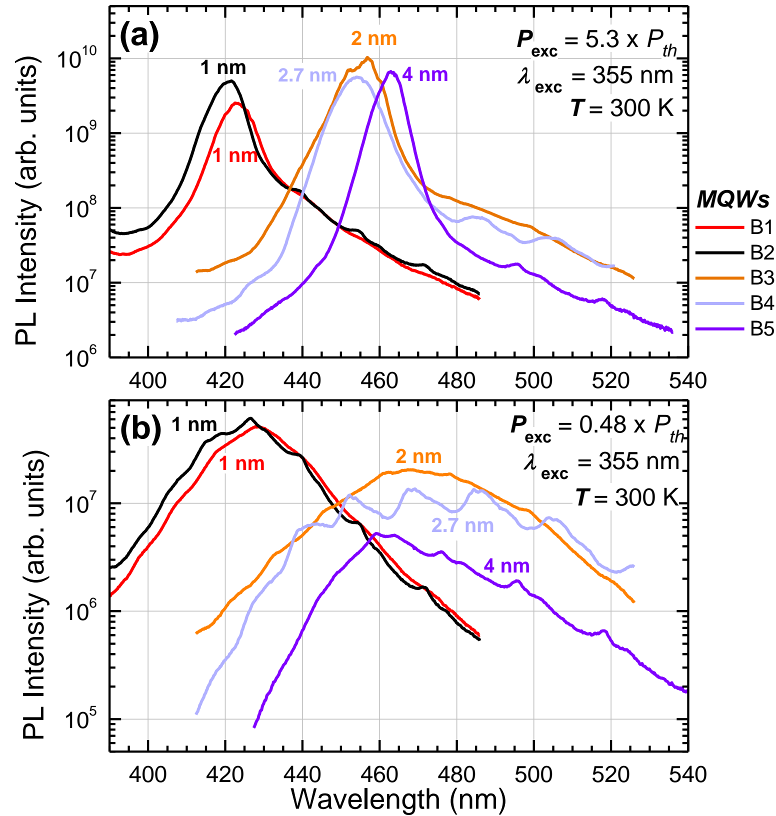

Fig. 7. PL spectra of the studied samples from group B under excitation power density above (a) and below (b) SE threshold. Next to each of the spectra a QW width in the according sample is provided.

To better compare the obtained results, a more detailed analysis of the excitation-dependent measurement results will be performed separately for epilayers and MQWs.

3.2 MQWs

The estimated PL efficiencies of all MQW samples are shown in Fig. 8. All samples under study showed an increase of PL efficiency with excitation followed by the saturation and decrease of PL efficiency up to the SE threshold value. PL efficiency droop is a characteristic property of InGaN-based structures, origin of which is usually attributed to Auger recombination[31], however, other explanations are also found in the literature.[32] Once the excitation power density exceeds the SE threshold, population inversion is achieved and SE becomes the dominant emission process leading to the steep increase of PL efficiency. At the highest excitations, a PL efficiency again starts to saturate, which is followed by a decrease of PL efficiency. This could be attributed to saturation of optical gain. Furthermore, for several samples a sharp drop in PL efficiency was evidenced at excitation power densities exceeding 9 MW/cm^2 due to laser induced optical damage of the sample.

PL efficiencies of sample group A (Fig. 8(a)) revealed that high efficiency of spontaneous emission results in a lower SE threshold. At excitation conditions below SE threshold, the highest PL efficiency was found for sample A4 with an In content of 12 %. This sample also shows the lowest SE threshold of 126 kW/cm^2. All other samples demonstrated lower efficiencies of SP emission and consequently, SE thresholds above 200 kW/cm^2, visible as critical points in the PL efficiency behaviour. The dependence of the estimated SE threshold values on the In percentage for this sample group is presented in Fig. 9(a). Increasing In content in the alloy leads to larger local compositional fluctuations, consequently increasing the density of the band tail states. Therefore, large amount of In in the alloy results in a strong localization of carriers in the sample. This reduces carrier mobility and non-radiative recombination as carriers are less likely to be trapped by defects. As a result, we observe a decrease of SE threshold values with increasing In content up to 12 %. One could assume that further increase of In percentage should result in even lower thresholds, however, the obtained results suggest otherwise. SE threshold increased 1.7 times while the amount of In increased from 12 % to 17 %. This could be explained in terms of structural quality of the sample. InGaN layers with high In content are known to show poor structural quality and high density of defects.[33] Therefore, higher carrier densities are required to reach population inversion and cause SE band.

Fig. 8(b) shows PL efficiencies of group B samples having different QW width. At the excitation power densities below the lowest SE threshold (485.8 kW/cm^2) samples with a narrow QW width (1 nm) showed the highest PL efficiency. Increased QW width leads to lower PL efficiencies in this range. This agrees well with the fact that wider QW widths result in higher QCSE and low overlap of electron and hole wave functions, which results in lower PL efficiency. However, for the sample group B, a higher SP efficiency does not result in a lower SE threshold as was evidenced for sample group A. In fact, the opposite effect is observed. Sample with the widest QW width and the lowest

SP emission efficiency exhibited the lowest SE threshold. The SE threshold dependence on QW width is presented in Fig. 9(b). SE threshold values slowly decreased with increasing QW widths up to 3 nm, however, sample B4 with the QW width of 4 nm showed significantly lower SE threshold (486 kW/cm^2). As SE band appears at high excitation power densities, previously discussed QCSE, which is more pronounced in wide QWs, should not influence the SE threshold. However, increased QW width results in an improved confinement of the electron wave function inside the QW[21]. In the finite QWs, electron wave function spreads into the barrier regions, which results in energy dissipation. This effect is more pronounced in the narrow QWs, therefore, higher excitation power densities are required to achieve population inversion in the narrow QWs. Enhanced electron wave function confinement in the wide QWs could be the main reason for lower SE thresholds obtained for the samples with wider QWs.

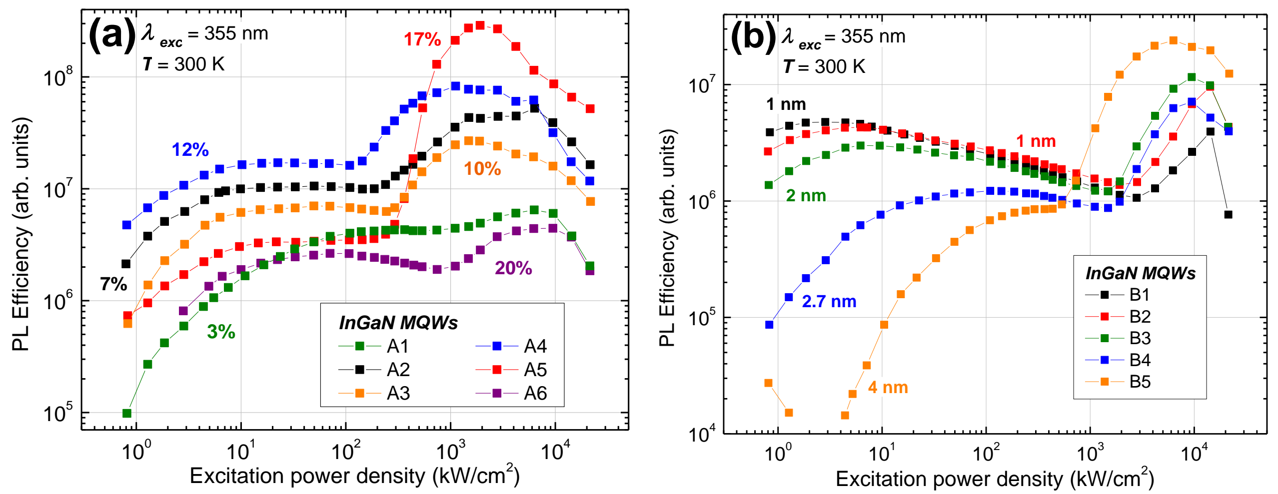

Fig. 8. Excitation-dependent PL efficiency of MQW samples which differed in In content (a) and QW width (b).

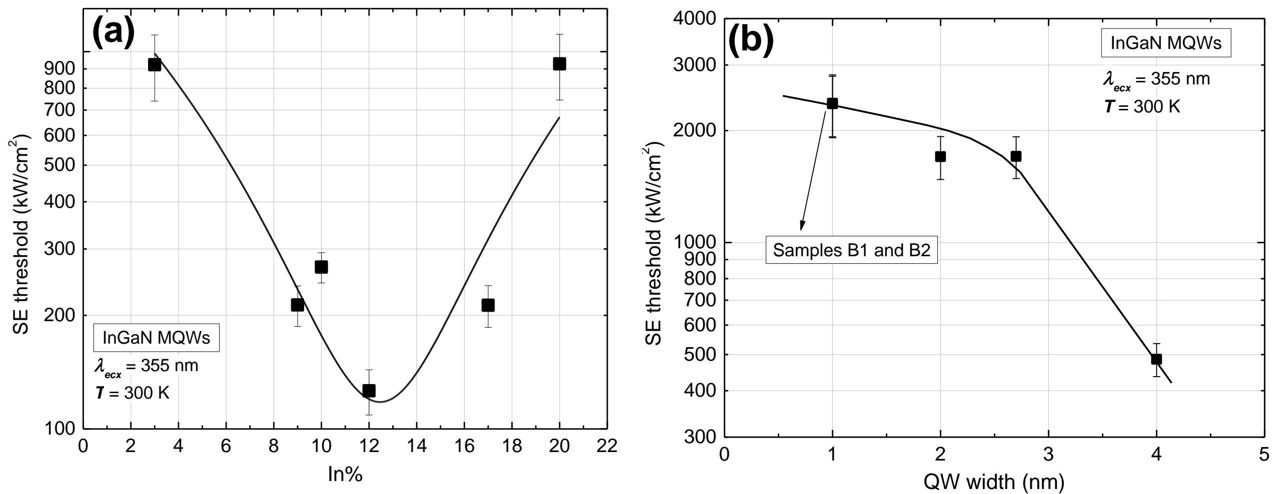

Fig. 9. Stimulated emission threshold dependence on In % (a) and QW width (b). Solid lines are a guide for an eye.

3.3 EPILAYERS

Obtained excitation-dependent spectra for the sample E4, which had the lowest SE threshold, are displayed in Fig. 10(a). As in the previous case, the inset of the graph (Fig. 10(a)) shows the PL efficiency dependence on excitation. The excitation power density at which the SE band appeared in the spectra matches well with the critical point in the excitation-dependent behavior of PL efficiency. Similar results were obtained for all studied samples. However, samples E6, E7 and E8 showed no SE band even at the highest excitations. Fig. 10(b) shows the comparison of excitation-dependent PL efficiencies of epilayer samples. Samples in which population inversion was not reached, demonstrated only saturation of PL efficiency followed by a decrease of PL efficiency in the high excitation region (>200 kW/cm^2), which indicates an efficiency droop effect discussed in the previous chapter. Therefore, it was assumed that the SE threshold of these samples exceeds 20 MW/cm^2 and they won't be included in the further discussion.

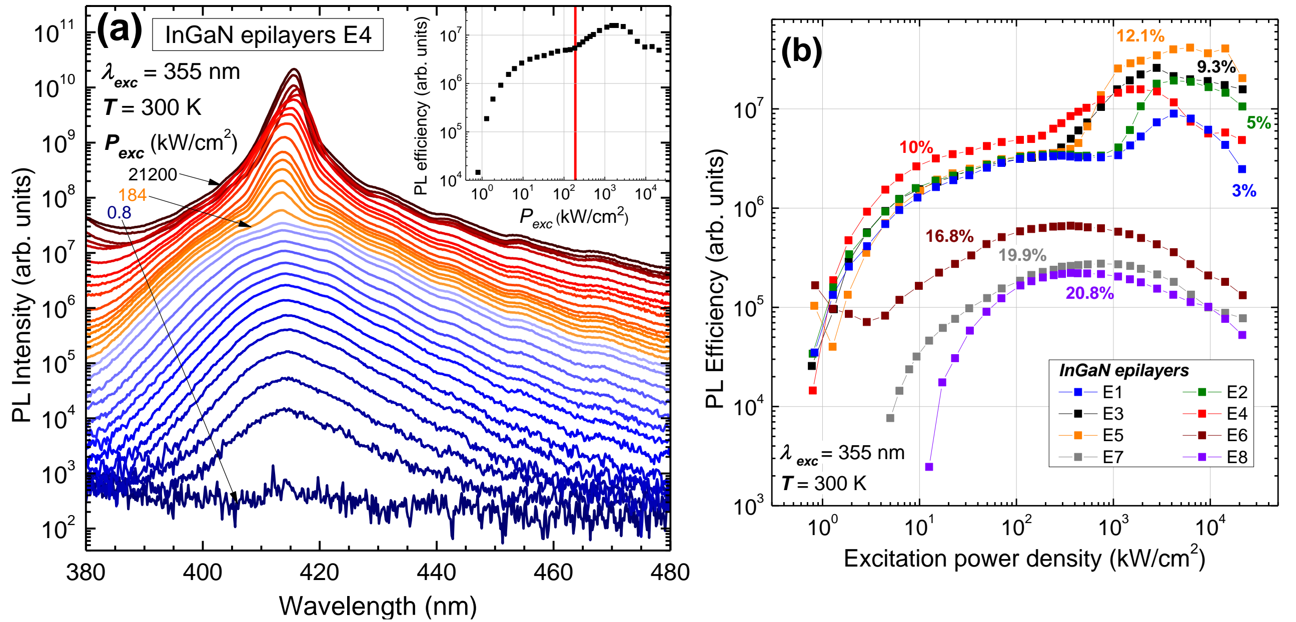

Fig. 10. Excitation-dependent PL spectra of sample E4 (a) and PL efficiency dependence on excitation for all samples from group E (b). Inset of the graph (a) shows the PL efficiency dependence on the excitation power density.

Estimated SE thresholds are depicted in Fig. 11. Generally, higher SE thresholds for epilayer structures compared to MQWs could be caused by the diffusion of carriers to the depth of the layer. However, the thickness of the epilayers studied in this work does not exceed 58 nm, which is rather thin, therefore, diffusion to the layer depth does not play an important role in this case. This results in comparable SE thresholds of epilayer structures and MQWs with increasing In content up to 10 %. On the other hand, even though MQW structures showed the lowest SE threshold when the In content was 12 %, sample E5 with in content of 12 % already showed about 2 times higher SE threshold than

the sample E4 with 10 % of In. This indicates that the epilayer structures generally have a worse structural quality than MQW structures, which could be the result of strain relaxation and higher density of defects.[33]

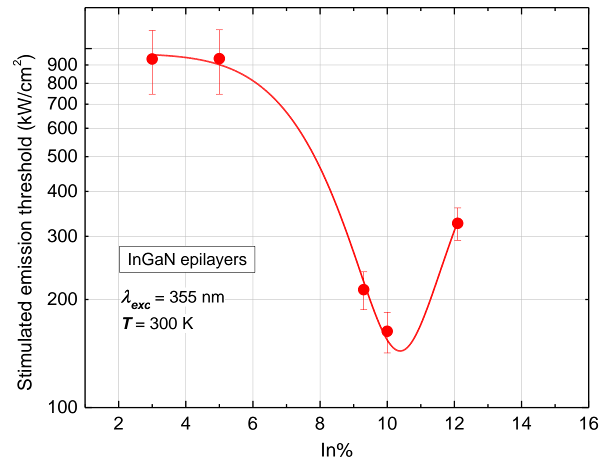

Fig. 11. SE threshold dependence on In % in epilayer structures.
Solid line is a guide for an eye.

3.4. PEAK POSITIONS OF SP EMISSION AND SE BANDS

As was already seen in the results of excitation-dependent PL measurements, SP band showed a peak shift from low to high excitation power densities. However, the comparison of such peak position shifts in MQW and epilayer structures revealed three different tendencies. For MQW structures, the magnitude of the SP emission peak position shift is influenced by both indium content and QW width. Peak shift increase with In content for MQW structures can be explained in terms of built-in electric field. Theoretical predictions of built-in field suggest that built-in field increases with increasing amount of In in the compound. As built-in fields are screened at high excitation power densities, larger built-in fields would result in larger peak position shifts of spontaneous emission. Such case observed in Fig. 12(a), which presents the peak position shift as the excitation is increased from the lowest up to the SE threshold. Larger QW widths also result in higher peak position shifts as QCSE dominates the emission process in the wide wells. However, sample B5 with the widest well showed a smaller SP emission peak positon shift than sample B4. This could be caused by a significantly lower SE threshold of sample B5 compared to other group B samples. As built-in electric field is not present in InGaN epilayer structures, samples from group E showed a very minor SP emission peak shifts compared to MQW structures.

Excitation-dependent results also showed that SE band appears on the high-energy slope of the SP emission band. This suggests that the SE originates from the localized states.[22,23] Fig. 12(b) shows

the PL peak position difference between the SE band and SP emission band for all samples in which population inversion was achieved. The peak position difference increases with In content in the sample. Larger In content in the sample leads to an increased density of the band-tail states. At low excitations carriers occupy the lowest localized states and increasing excitation power density results in the band-filling effect. SE occurs when carriers occupy the states near the mobility edge, therefore, the increased density of the band-tail states in samples with high In content could be the main reason for the larger difference between the peak positions of SE band and SP emission band. However, the dependence of peak position difference on QW width is more complex. Peak shift values increase with increasing QW width except for sample B5. In fact, sample B5 showed the lowest difference between the peak positions of SE band and SP emission band (37 meV) which again could be attributed to the lower SE threshold of sample B5 compared to other samples from group B. Meanwhile, peak position differences obtained for epilayer samples (group E) do not reveal a clear correlation with In content in the alloy, although the increasing trend might be assumed.

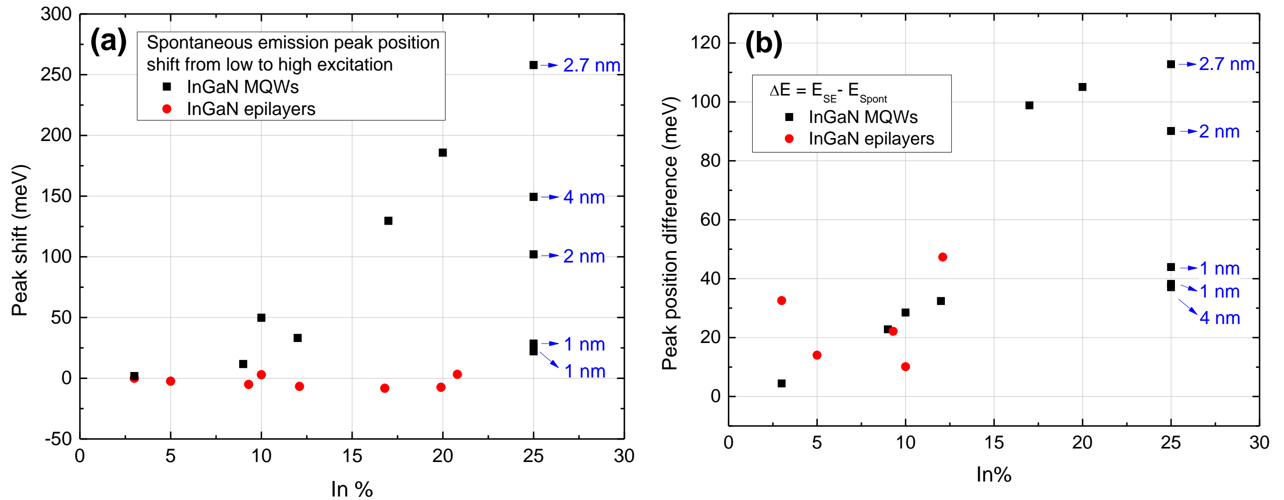

Fig. 12. Spontaneous emission peak position shift from low to high excitation power density (a), PL peak position difference between SE band and SP emission band (b). Blue numbers in the graph represent the QW width in the group B samples.

3.5 OPTICAL GAIN IN MQWs

To evaluate the optical gain in the MQW samples from group B, VSL technique was used to measure the PL spectra at excitation stripe lengths ranging from 25 μm to 5000 μm. For all samples under study the excitation power density was chosen to be three times greater than the estimated SE threshold ($3 \times P_{th}$). The typical results of such measurements are presented in Fig. 13(a) for sample B1. The smallest step in excitation stripe length was 2.5 μm, however, for a better clarity of the Fig. 13(a), only part of the measured spectra with a larger step in excitation stripe length (defined in

Fig. 13(a)) is presented in the figure. At the lowest excitation stripe lengths only the amplified spontaneous emission (ASP) band was evidenced, intensity of which steeply increased with the excitation stripe length. At the excitation stripe lengths exceeding 1350 μm, another narrow band appeared on the high energy side of the ASP band. Such PL spectra behaviour was evidenced for all samples under study. Fig. 13(b) shows the integrated PL intensity dependence on the excitation stripe length estimated for all studied samples. It can be clearly seen that the range of excitation stripe lengths at which the initial steep rise of PL intensity was evidenced differed among the studied samples. For samples with wide QW widths (B4 and B5) PL intensity increased at smaller excitation stripe lengths than for samples with narrower QW widths. To better understand the emission processes behind such PL intensity behaviour and evaluate the gain coefficient, these dependences were analysed individually.

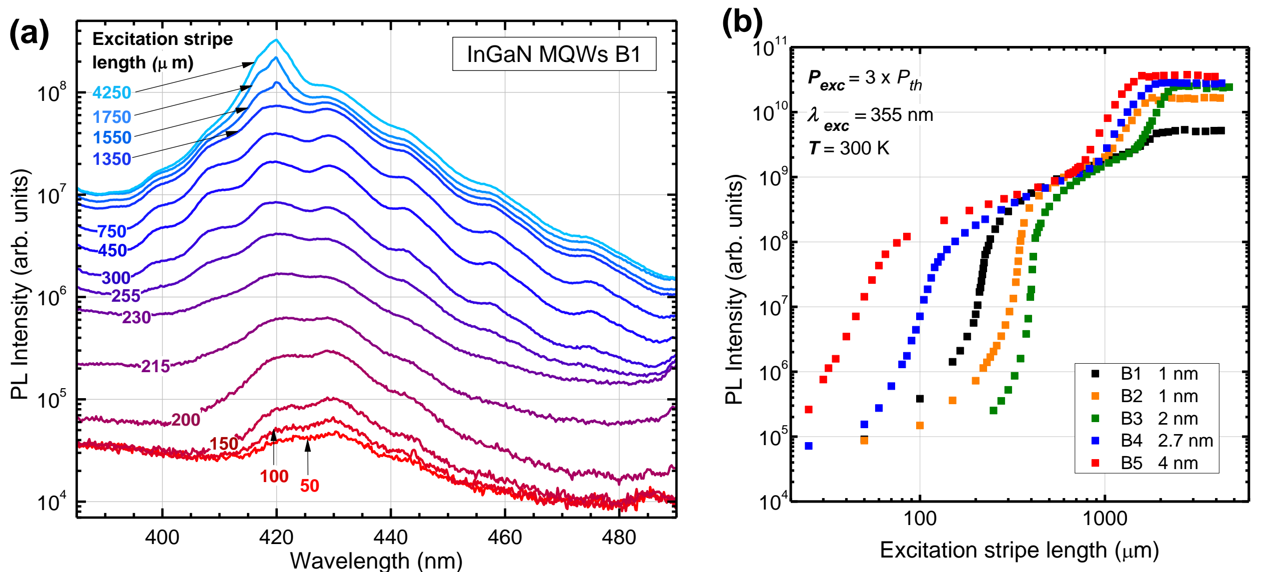

Fig. 13. PL spectra of sample B1 measured at different excitation stripe lengths (a) and integrated PL intensity dependence on the excitation stripe length for all group B samples (b).

Fig. 14(a) shows the integrated PL intensity dependence on excitation stripe length for sample B4. First, a steep exponential increase in PL intensity was observed with excitation stripe lengths up to 150 μm. This was followed by a gradual increase in PL intensity up to 900 μm. Once the excitation stripe length exceeds 900 μm, another sudden increase of PL intensity was evidenced which was followed by the saturation of PL intensity up to the highest excitation stripe lengths. The rapid exponential increase in PL intensity could be attributed to ASP, which starts to saturate at excitation stripe lengths exceeding 150 μm. Saturation of ASP is caused by the depletion of the excited state population. Therefore, further increase in excitation stripe length results in a much slower rise of PL intensity. A second steep increase of PL intensity occurs once a critical excitation stripe length is

reached. At this critical excitation stripe length also a narrow band appeared on the high energy side of the ASP. Complete saturation of PL intensity at the highest excitation stripe lengths most probably indicates that the actual excitation stripe does not increase any more.

To evaluate the optical gain parameter, the initial rise of PL intensity dependence on the excitation stripe length was fitted using two different approaches:

$$I(l) = \frac{I_s}{g}(e^{gl} - 1), \tag{1}$$

where I_s is the spontaneous emission intensity, g is the is the unsaturated gain coefficient and l is the excitation stripe length. A second approach includes a gain saturation factor:

$$I(l) = \frac{I_{ss}}{(1+Ce^{-gl})} + \frac{I_{ss}}{(1+C)}, \tag{2}$$

where I_{ss} is the saturation intensity, C is the saturation coefficient. The best fits obtained by these expressions for sample B4 are presented in the Fig. 14(a). A second approach allows to fit a slightly wider range of values, however, both approaches do not describe the further behaviour of PL intensity. Optical gain coefficients obtained from the fits based on the first approach and SE thresholds obtained from excitation-dependent measurements are presented in Fig. 14(b). Results suggest that increased QW width leads to a higher optical gain coefficient and, consequently, a lower SE threshold. In case of higher optical gain coefficients, there is a bigger probability that spontaneously emitted photon will induce another radiative transition, therefore, a lower excitation power density is required to achieve SE band.

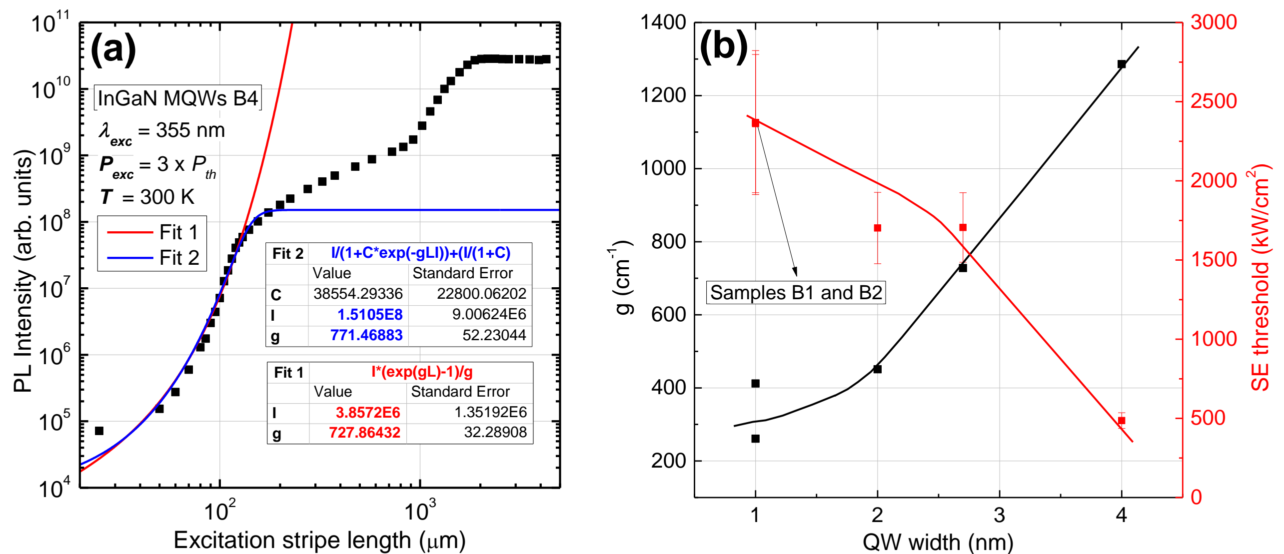

Fig. 14. Integrated PL intensity dependence on the excitation stripe length for sample B4 (a). The optical gain coefficient and SE threshold dependence on QW width (b). Solid lines (b) are a guide for an eye.

4. CONCLUSIONS

1. SE threshold for MQW structures decreases with In content up to 12% indicating that decreasing SE threshold values are a result of effective carrier localization. However, in case of large In content (17-25%) SE is governed by high defect densities and poor structural quality of the samples, which results in high SE threshold. On the other hand, larger QW width in high-In-content samples decreased the SE threshold, which was attributed to better electron wave function confinement in the QW.

2. Epilayer structures showed a similar SE threshold dependence on In content as the MQW structures, however, the SE threshold started to increase at lower In content (12%) compared to MQW structures, indicating lower structural quality of epilayer structures. Samples with large In content (17-21%) showed no SE band even at the highest excitations.

3. The lowest difference between the peak positions of SP emission and SE bands for MQW structures was 4 meV obtained for sample with In content of 3% and increased up to 186 meV for sample with 20% of In in the alloy. Such behavior was attributed to an increasing density of the band tail states. Large In content also leads to a stronger influence of built-in electric field in the MQWs, which results in the pronounced shift of SP emission band with increasing excitation.

4. For MQW samples with different QW width, the highest optical gain coefficient was 1300 cm^{-1} obtained for sample with the widest QW width (4 nm), which also showed the lowest SE threshold. Optical gain coefficients obtained for MQW structures increase with QW width, which leads to lower SE thresholds for wider QWs.

REFERENCES

1. Wang, W.-J. *et al.* Enhancing performance of GaN-based LDs by using GaN/InGaN asymmetric lower waveguide layers. *Chin. Phys. B* **31**, 074206 (2022).
2. Alahyarizadeh, G. *et al.* Effect of different EBL structures on deep violet InGaN laser diodes performance. *Opt. Laser Technol.* **76**, 106–112 (2016).
3. Hardy, M. T. *et al.* Group III-nitride lasers: a materials perspective. *Mater. Today* **14**, 408–415 (2011).
4. Auf Der Maur, M. *et al.* Efficiency Drop in Green InGaN/GaN Light Emitting Diodes: The Role of Random Alloy Fluctuations. *Phys Rev Lett,* **116**, 207401 (2016).
5. Alahyarizadeh, G. *et al.* Analytical and visual modeling of InGaN/GaN single quantum well laser based on rate equations. *Opt. Laser Technol.* **44**, 12-20 (2012).
6. Kojima, K. *et al.* Inhomogeneously broadened optical gain spectra of InGaN quantum well laser diodes. *Phys. status solidi c,* **5**, 2126–2128 (2008).
7. Qin, H. *et al.* Mechanical, Thermodynamic and Electronic Properties of Wurtzite and Zinc-Blende GaN Crystals. *Mater.* **10**, 1419 (2017).
8. Paisley, M. J. *et al.* Growth of cubic phase gallium nitride by modified molecular-beam epitaxy. *J. Vac. Sci. Technol. A Vacuum, Surfaces, Film.* **7**, 701 (1998).
9. Menniger, J. *et al.* Identification of optical transitions in cubic and hexagonal GaN by spatially resolved cathodoluminescence. *Phys. Rev. B* **53**, 1881 (1996).
10. Vurgaftman, I. *et al.* Band parameters for III-V compound semiconductors and their alloys. *J. Appl. Phys.* **89**, 5815 (2001).
11. Wu, J. *et al.* Temperature dependence of the fundamental band gap of InN. *J. Appl. Phys.* **94**, 4457 (2003).
12. Chen, Y. *et al.* GaN buffer growth temperature and efficiency of InGaN/GaN quantum wells: The critical role of nitrogen vacancies at the GaN surface. *Appl. Phys. Lett.* **118**, 111102 (2021).
13. Wu, J. When group-III nitrides go infrared: New properties and perspectives. *J. Appl. Phys.* **106**, 011101 (2009).
14. Oliver, R. A. *et al.* Growth modes in heteroepitaxy of InGaN on GaN. *J. Appl. Phys.* **97**, 013707 (2004).
15. Du, C. *et al.* Enhancing the quantum efficiency of InGaN yellow-green light-emitting diodes by growth interruption. *Appl. Phys. Lett.* **105**, 071108 (2014).
16. Li, G. *et al.* GaN-based light-emitting diodes on various substrates: a critical review. *Reports Prog. Phys.* **79**, 056501 (2016).

17. Hangleiter, A. *et al.* Suppression of Nonradiative Recombination by V-Shaped Pits in GaInN/GaN Quantum Wells Produces a Large Increase in the Light Emission Efficiency. *Phys Rev Lett,* **95**, 127402 (2005).

18. Ryou, J. H. *et al.* Control of quantum-confined stark effect in InGaN-based quantum wells. *IEEE J. Sel. Top. Quantum Electron.* **15**, 1080–1091 (2009).

19. Nakamura, S. *et al.* InGaN-based multi-quantum-well-structure laser diodes. *Japanese J. Appl. Physics,* **35**, L74 (1996).

20. Shang, Z. J. *et al.* Carrier thermalization under stimulated emission in In0.17Ga0.83N epilayer at room temperature. *Appl. Phys. Lett.* **105**, 232104 (2014).

21. Wang, T., Parbrook, P. J., Whitehead, M. A., Fan, W. H. & Fox, A. M. Study of stimulated emission from InGaN/GaN multiple quantum well structures. *J. Cryst. Growth* **273**, 48–53 (2004).

22. Schmidt, T. J. *et al.* Stimulated emission characteristics of InGaN/GaN multiple quantum wells: Excitation length and excitation density dependence. *Appl. Phys. Lett.* **73**, 3689 (1998).

23. An, X. *et al.* Temperature and excitation dependence of stimulated emission and spontaneous emission in InGaN epilayer*. *Chinese Phys. B* **28**, 057802 (2019).

24. Shee, S. K. *et al.* MOCVD growth, stimulated emission and time-resolved PL studies of InGaN/(In)GaN MQWs: Well and barrier thickness dependence. *J. Cryst. Growth* **221**, 373–377 (2000).

25. Özgür, Ü., Everitt, H. O. & Keller, S. Stimulated emission and ultrafast carrier relaxation in InGaN multiple quantum wells. *Appl. Phys. Lett* **82**, 1416 (2003).

26. Nakamura, S. *et al.* Influence of excitation power and temperature on photoluminescence in InGaN/GaN multiple quantum wells. *Opt. Express, Vol. 20, Issue 4, pp. 3932-3940* **20**, 3932–3940 (2012).

27. Eliseev, P. G., Perlin, P., Lee, J. & Osiński, M. “Blue” temperature-induced shift and band-tail emission in InGaN-based light sources. *Appl. Phys. Lett.* **71**, 569 (1998).

28. Shaklee, K. L. *et al.* Optical gain in semiconductors. *J. Lumin.* **7**, 284–309 (1973).

29. Hader, J. *et al.* Influence of internal fields on gain and spontaneous emission in InGaN quantum wells. *Appl. Phys. Lett.* **89**, 171120 (2006).

30. Xu, G. *et al.* Investigation of large Stark shifts in InGaN/ GaN multiple quantum wells. *J. Appl. Phys* **113**, 33104 (2013).

31. Shen, Y. C. *et al.* Auger recombination in InGaN measured by photoluminescence. *Appl. Phys. Lett.* **91**, 141101 (2007).

32. Verzellesi, G. *et al.* Efficiency droop in InGaN/GaN blue light-emitting diodes: Physical mechanisms and remedies. *J. Appl. Phys.* **114**, 071101 (2013).

33. Bazioti, C. *et al.* Defects, strain relaxation, and compositional grading in high indium content InGaN epilayers grown by molecular beam epitaxy. *J. Appl. Phys* **118**, 155301 (2015).

Priverstinė spinduliuotė ir optinis stiprinimas InGaN dariniuose

Aleksandra Širvinskytė

Santrauka

InGaN yra plačiai taikoma medžiaga kietakūniame apšvietime. InGaN/GaN kvantinės duobės (MQWs), kaip aktyvioji sritis, leido sukurti aukšto emisijos efektyvumo šviestukus bei yra plačiai pritaikoma lazerinių diodų (LD) gamyboje. Šios medžiagos patrauklumą lėmė galimybė varijuoti InGaN draustinį energijų tarpą, keičiant In ir Ga santykį lydinyje. Tačiau, InN ir GaN medžiagų skirtumai lemia komplikuotą InGaN auginimą. InGaN bandiniai su dideliu In kiekiu pasižymi prastesne bandinio kokybe, didesniu defektų tankiu. Bandinių parametrai taip pat lemia krūvininkų lokalizaciją bandinyje bei vidinio elektrinio lauko įtaką spindulinei krūvininkų rekombinacijai. Siekiant įveikti šiuos sunkumus bei pagerinti priverstinės spinduliuotės efektyvumą InGaN struktūrose, moksliniai tyrimai yra sutelkti į InGaN auginimo sąlygų optimizavimą, bei priverstinės spinduliuotės parametrų gerinimą.

Šiame darbe buvo tiriama priverstinės spinduliuotės parametrų priklausomybė nuo kvantinės duobės pločio ir In procento bandiniuose. Buvo tirtos trys bandinių grupės, kurių bandiniai pasižymėjo skirtinga struktūra. Aktyviąją bandinių sritį sudarė arba InGaN/GaN kvantinės duobės, arba InGaN epitaksiniai sluoksniai. Taip pat, bandiniai pasižymėjo skirtingu In kiekiu lydinyje arba kvantinės duobės pločiu. Siekiant įvertinti priverstinės spinduliuotės slenkstį bandiniuose, fotoliuminescencijos (FL) matavimai buvo atlikti plačiame žadinimo galios tankių intervale. Taip pat, buvo atlikti FL matavimai remiantis kintamo žadinančios juostelės ilgio (VSL) metodu ir įvertintas optinio stiprinimo koeficientas bandiniuose.

Buvo pastebėta, kad didinant In kiekį bandinyje iki 12 % pasiekiamos vis žemesnės priverstinės spinduliuotės slenksčio vertės dėl efektyvios krūvininkų lokalizacijos. Tačiau didesni In kiekiai bandinyje gali lemti prastesnę bandinių kokybę, dėl kurios priverstinės spinduliuotės slenkstis pradeda sparčiai augti. Panaši tendencija stebima ir epitaksinių sluoksnių bandiniuose, tačiau kritinė In kiekio bandinyje vertė, ties kuria priverstinės spinduliuotės slenkstis ima augti, yra žemesnė (12%). Tai reiškia, jog epitaksiniai sluoksniai su didesniais In kiekiais pasižymi prastesne bandinio kokybe. Priverstinės spinduliuotės slenkstis taip pat priklauso nuo kvantinės duobės pločio. Geresnis elektrono banginės funkcijos apribojimas platesnėse kvantinėse duobėse lemia mažesnes priverstinės spinduliuotės slenksčio vertes bandiniams su platesnėmis kvantinėmis duobėmis. Taip pat pastebėta, jog skirtumas tarp priverstinės spinduliuotės ir spontaninės spinduliuotės juostų piko padėčių didėja su didėjančiu In procentu lydinyje dėl būsenų tankio uodegos išplitimo. Didžiausias optinio stiprinimo koeficientas (1300 cm^{-1}) gautas bandiniui B5, kuris pasižymėjo plačiausiu kvantinės duobės pločiu (4 nm).